Earthquake spectra and near-source attenuation in the Cascadia subduction zone

J. Gomberg,[1] K. Creager,[2] J. Sweet,[2] J. Vidale,[2] A. Ghosh,[3] and A. Hotovec[2]

Received 23 November 2011; revised 27 February 2012; accepted 13 April 2012; published 23 May 2012.

[1] Models of seismic source displacement spectra are flat from zero to some corner frequency, f_c, regardless of source type. At higher frequencies spectral models decay as f^{-1} for slow events and as f^{-2} for fast earthquakes. We show that at least in Cascadia, wave propagation effects likely control spectral decay rates above ~2 Hz. We use seismograms from multiple small-aperture arrays to estimate the spectral decay rates of near-source spectra of 37 small 'events' and find strong correlation between source location and decay rate. The decay rates (1) vary overall by an amount in excess of that inferred to distinguish slow sources from fast earthquakes, (2) are indistinguishable for sources separated by a few tens of km or less, and (3) separate into two populations that correlate with propagation through and outside a low-velocity zone imaged tomographically. We find that some events repeat, as is characteristic of low-frequency earthquakes (LFEs), but have spectra similar to those of non-repeating earthquakes. We also find no correlation between spectral decay rates and rates of ambient tremor activity. These results suggest that earthquakes near the plate boundary, at least in Cascadia, do not distinctly separate into 'slow' and 'fast' classes, and correctly accounting for propagation effects is necessary to characterize sources.

Citation: Gomberg, J., K. Creager, J. Sweet, J. Vidale, A. Ghosh, and A. Hotovec (2012), Earthquake spectra and near-source attenuation in the Cascadia subduction zone, *J. Geophys. Res.*, *117*, B05312, doi:10.1029/2011JB009055.

1. Introduction

[2] It is generally accepted that spectral characteristics distinguish slow seismic sources from those of ordinary or fast earthquakes. The signatures of seismic events associated with slow slip include discrete, pulse-like, low frequency earthquakes (LFEs) or very low frequency earthquakes (VLFs) and emergent, long-duration tremor that may be built out of superposed repeating LFE signals [*Ito et al.*, 2007; *Brown et al.*, 2009]. Theoretical models of displacement wave amplitude spectra are flat from zero to some corner frequency, f_c, regardless of source type. At higher frequencies spectral models decay as f^{-1} for slow events [*Ide et al.*, 2007; *Rubinstein et al.*, 2007; *Shelly et al.*, 2007; *Ide*, 2010] and as f^{-2} according to the classic 'Brune' model of fast earthquakes [*Brune*, 1970].

[3] In this study we refer to the sources responsible for all the aforementioned seismic signals, including those considered to be standard earthquakes, as 'events'. We use seismograms from multiple small-aperture arrays (Figure 1) to estimate the spectral decay-rates of near-source spectra of 37 small events and examine their correlations with tomographically imaged seismic velocity structure [*Rondenay et al.*, 2001; *Preston*, 2003; *Abers et al.*, 2009; *Calkins et al.*, 2011; *Calvert et al.*, 2011]. Although not our primary focus, we also examine the degree to which events repeat because, as noted above, repeating is a characteristic of LFEs that comprise tremor [*Ito et al.*, 2007; *Brown et al.*, 2009]. Our results suggest that earthquakes near the plate boundary, at least in Cascadia, do not distinctly separate into 'slow' and 'fast' classes, and correct accounting for propagation effects is necessary to characterize sources.

2. Data

[4] In Cascadia a low rate of earthquakes near the plate boundary and a paucity of identifiable LFEs [*Ide*, 2010], despite an abundance of tremor, are clear differences from other subduction zones and present challenges to studying the processes underlying slow to fast slip events. New data from five seismic micro-arrays permit us to address these challenges and to investigate these differences. The arrays were deployed, on and off, between June 2009 and September 2011 in northern Washington, with 10–20 3-component seismographs in each array spread over apertures of 1–2 km (Figure 1). The seismographs recorded ground velocity sampled at 50 Hz. Most stations used short-period L-28 sensors but some had broadband sensors, with responses that are flat to velocity above 4.5 Hz and 0.03 Hz, respectively.

[1]U.S. Geological Survey, University of Washington, Seattle, Washington, USA.
[2]Earth and Space Sciences, University of Washington, Seattle, Washington, USA.
[3]Earth and Planetary Sciences, University of California, Santa Cruz, California, USA.

Corresponding author: J. Gomberg, U.S. Geological Survey, University of Washington, Seattle, WA 98195, USA. (gomberg@usgs.gov)

0148-0227/12/2011JB009055

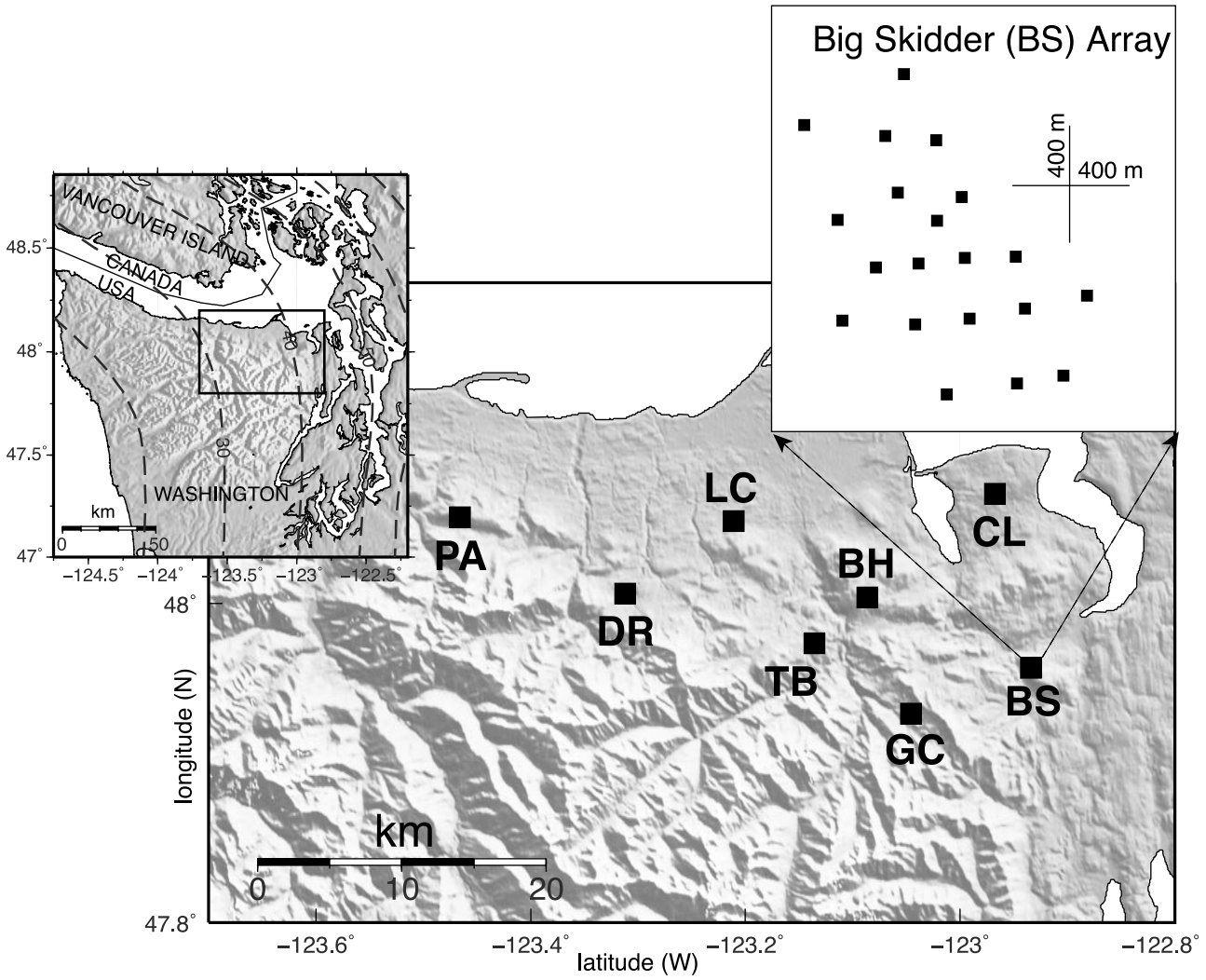

Figure 1. Map of northern Washington and array locations. The locations of each array, labeled with the codes used for corresponding station names, are superposed on shaded topography. Water shown as white areas. Left inset shows map location (box) within northern Cascadia with contoured depths to the plate interface determined by *McCrory et al.* [2006] (km, dashed lines). Right inset shows example array layout, for one of the arrays.

We used data from both sensor types, deconvolving the corresponding instrument responses as part of the processing. We restricted our analyses to frequencies between 2 and 16 Hz because outside this range the noise amplitudes generally became comparable to those in the signals, based on comparisons of spectra of pre-event noise and signals (see Figure S1 of the auxiliary material).[1] The low frequency limit is due to the L-28 response decreasing below 4.5 Hz, but the high frequency limit of ~16 Hz is where the signal becomes smaller than the ground noise. The latter sets an intrinsic limit on the maximum frequency that can be examined for events of these small sizes.

[5] Detection algorithms tailored for these data permitted identification of 37 events with magnitudes in the approximate range $-1.5 \leq M \leq 1.5$, most with distinct P- and S-wave arrivals (Table 1 and Figure 2). Most events were classified initially as ordinary earthquakes using the procedure described in *Vidale et al.* [2011], which involved a combination of an automated detection scheme based on ratios of short-term to long-term average signal levels and visual verification. The signals for these events were temporally isolated, each had both clear P- and S-waves, and their spectral content or recurrence was not considered. Some other events were first classified as LFEs based on their repeating occurrence in the study of *Sweet et al.* [2010], which employed an algorithm that cross-correlates a template waveform with a moving window of a continuous data stream recorded at the same station, with repeats noted well outside the time window of this study. LFEs are identified as windows in which the correlation coefficients summed across 3-components of several stations exceeds a threshold value [*Sweet et al.*, 2010]. After discovering that several of our events were identified in both the *Vidale et al.* [2011]

[1]Auxiliary materials are available in the HTML. doi:10.1029/2011JB009055.

Table 1. Event Characteristics

Event	Yr/Mo/Dy	Hr:Min:Sec	Lat. (°N)	Lon. (°W)	Depth (km)	Repeats?	Peak Amp.	Quality
1	2010/03/01	1:34:42.87	47.63	−123.31	31.8		45	2
2	2010/03/08	20:01:22.32	48.15	−123.06	42.9		128	3
3	2010/03/10	5:54:29.11	48.28	−123.55	36.7		239	2
4	2010/03/13	6:13:08.14	48.19	−123.08	36.9		113	3
5	2010/03/13	11:36:13.06	47.80	−123.02	46.6		15	2
6	2010/03/17	12:31:12.84	47.96	−123.10	50.8		855	1
7	2010/03/18	4:08:17.36	47.90	−122.89	41.8	Y	118	5
8	2010/03/27	2:29:05.61	47.47	−123.12	34.4		12	2
9	2010/04/03	22:15:24.48	48.37	−122.89	42.9	Y (13)	266	2
10	2010/04/17	5:15:05.22	48.57	−123.13	42.8	Y (11)	224	2
11	2010/04/17	5:32:19.88	48.59	−123.15	39.8	Y (10)	172	2
12	2010/04/18	16:16:33.75	48.29	−123.32	46.0		118	1
13	2010/04/18	20:26:37.40	48.37	−122.90	41.8	Y (9)	424	2
14	2010/04/20	10:04:36.77	47.80	−122.79	55.7		993	1
15	2010/04/24	16:18:20.03	48.57	−123.12	38.6		164	1
16	2010/05/14	1:19:27.91	47.85	−123.57	35.4		62	2
17	2010/05/19	7:59:56.15	47.67	−123.13	38.3		20	2
18	2010/06/04	2:11:41.81	47.76	−122.70	49.9		138	2
19	2010/06/06	3:45:39.88	48.45	−123.56	34.2		86	2
20	2010/06/13	11:03:11.41	48.22	−123.12	35.0		89	2
21	2010/06/15	2:34:12.47	48.26	−123.16	45.7		35	2
22	2010/06/19	6:54:26.54	48.60	−123.12	49.4		102	2
23	2010/06/27	21:25:35.78	48.53	−123.61	39.5		246	1
24	2010/06/28	3:25:42.98	48.43	−123.37	34.3		62	1
25	2010/06/30	10:20:05.59	48.01	−123.19	46.6		137	2
26	2010/06/30	23:35:52.92	47.95	−122.55	47.1	Y	26	4
27	2010/07/16	5:09:49.66	48.31	−123.36	49.9		75	1
28	2010/07/28	13:53:24.37	47.82	−122.67	51.1		155	2
29	2010/08/03	8:36:02.55	48.40	−123.58	34.5		55	1
30	2010/08/07	21:34:38.00	48.32	−123.17	43.5		15	2
31	2010/08/10	15:45:15.34	48.35	−123.33	33.3		69	2
32	2010/08/16	6:31:39.39	48.06	−122.89	45.9		62	5
33	2010/08/19	9:57:13.77	47.92	−122.95	43.5		79	4
34	2010/08/26	13:14:38.29	47.73	−122.77	49.2		3989	1
35	2010/03/17	10:59:00.00	48.23	−122.76	39.0	Y	129	4
36	2010/03/07	00:56:00.00	47.90	−122.80	44.0	Y	17	4
37	2010/08/17	7:17:00.00	47.94	−123.04	40.0	Y	193	4

Events 1–34 were identified as earthquakes using procedures described in *Vidale et al.* [2011] and events 35–37 and 10 were initially identified as LFEs, based on the analyses described in *Sweet et al.* [2010]. Events with repeats among this suite of 37 events are indicated by the event number of the repeat in parentheses. Qualitative assessments of the reliability of spectral results for each event are numbered from 1 to 5 (right column). These assignments were based on the number of arrays that recorded an event and the signal-to-noise ratios in the 2–16 Hz passband. An event recorded on multiple arrays has 1 if all data are above noise, a 2 if some data are at/below the noise and a 4 if most data are only barely above the noise. Events recorded on only 1 array are assigned a 3 if all signals are above the noise and a 5 if most are barely above the noise. Peak amplitudes are the average peaks of the two horizontal components at station BH04 in units of counts, chosen because it recorded all events except Event 32, for which we list the value at station GC03 (only the GC array clearly recorded this event).

and the *Sweet et al.* [2010] studies we looked for repeats of all 37 events using the cross-correlation analysis over time intervals much longer than the period our study spans. 25% or more of these 37 events recurred multiple times over intervals from hours to years.

[6] For each earthquake we used all E-W recordings (overall this component had the highest signal-to-noise ratio) for which both P- and S-wave arrivals were visible. Results are nearly identical for the N-S components (Figure S2 of the auxiliary material shows comparisons). We extracted the S-wave signals within 0.5 s before and 2.5 s after the visually measured arrival time, measured spectra using the multitaper method supplied in the MATLAB software package, and converted to spectral displacement. Noise spectra were estimated by applying the same analysis to 3-s samples extracted just prior to the measured P wave arrival. The results presented are for spectra that were weighted by the corresponding mean noise amplitude, but noise weighting had insignificant effect on the results. See Figure S1 of the auxiliary material for plots of measured and fit spectra of all waveforms used and corresponding samples of pre-event noise.

3. Near-Source, Site, and Propagation Spectra

[7] We exploited the multiplicity of recording and source-array geometry (Figures 1 and 2) to separate the effects of local site response, regional propagation (attenuation and spreading) and processes near or at the source, with a minimum of assumptions and a priori parameterization. Our primary goal is to examine the variation between events among their near-source spectra rather than to constrain absolute spectral shape, which is more sensitive to hard-to-resolve model parameters.

3.1. Estimation Procedure

[8] We employed a procedure similar to that of *Andrews* [1986], *Hardebeck and Aron* [2009] and *Chen and Shearer* [2011] but with a simpler propagation model. The next few paragraphs summarize our approach, followed by a more

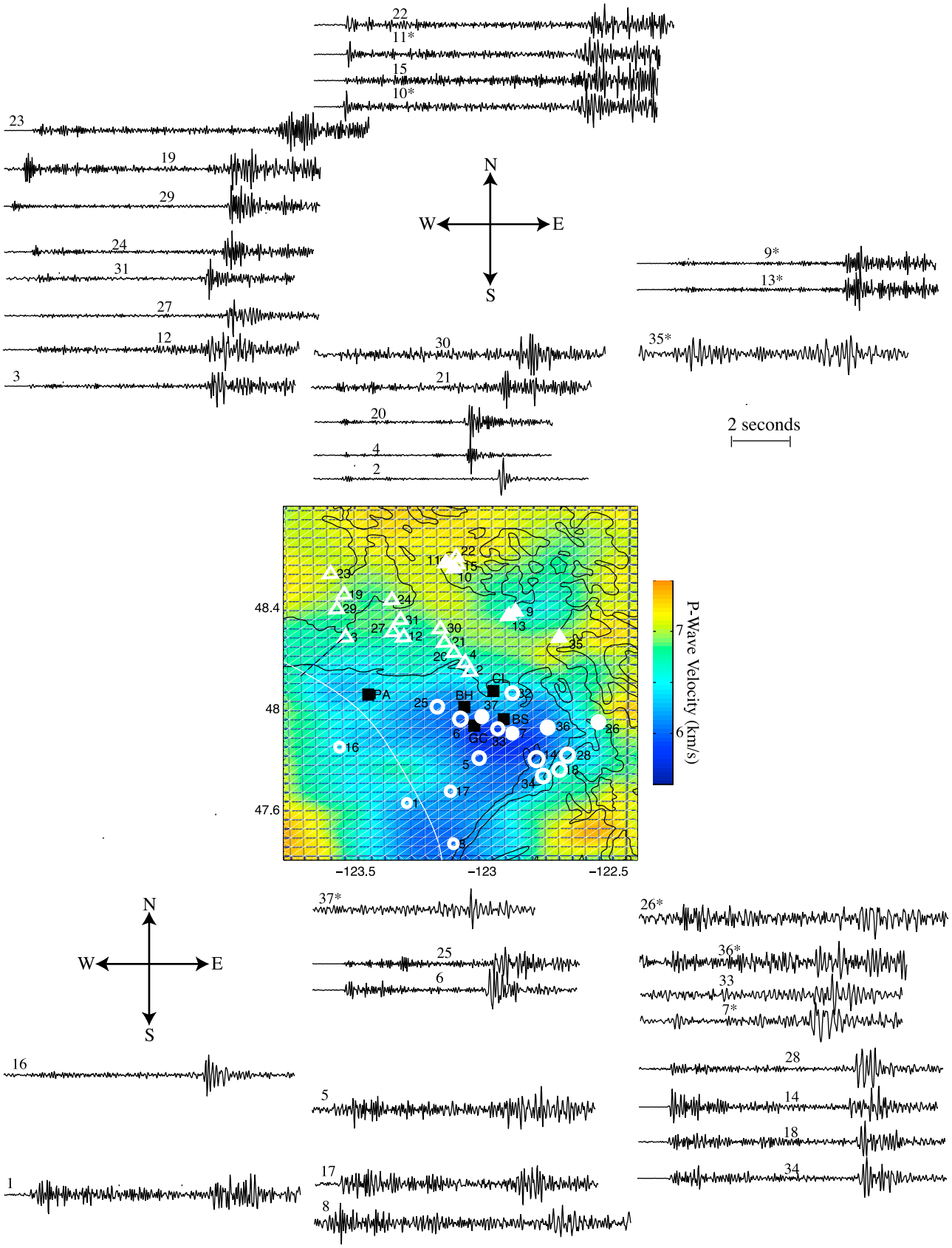
22
11*
15
10*
23
19
29
24
31
27
12
3
N
W
E
S
9*
13*
35*
30
21
20
4
2
2 seconds
48.4
48
47.6
−123.5
−123
−122.5
P-Wave Velocity (km/s)
7
6
PA
BH
CL
BS
GC
37*
25
6
26*
36*
33
7*
16
5
28
14
18
34
1
17
8

Figure 2

detailed explanation. All measured, modeled and noise spectra are shown in the auxiliary material. The modeled spectra do not fit the measured spectra precisely, and for some event-stations differ in certain passbands by factors of 3 or more. However, this is not surprising given the variability in site response, which at specific stations also seems to be event-dependent (see section 3.3 and Figures 4 and 5). Overall the modeled spectra reproduce smoothed versions of the measured spectra, but with sufficient resolution that preserves the essential features of the spectral variations. Our data consist of logarithms of spectral amplitudes for J earthquakes recorded at some or all of K arrays, each of which had up to $N(k)$ stations. We first fit the >1000 measured spectra simultaneously with a series of J lines, with a single unknown slope and J unknown intercepts. These represent the regionally averaged attenuation and J different event sizes plus any scaling common to all data, respectively.

[9] After removing estimated linear fits from the spectra we assumed the remaining spectral shapes were due to near-source effects and site response local to each receiver. The component of the shape common to all the spectra for each of the J events reflects near-source processes and those components common to each of the $N(k)$ stations reflect receiver site response. We find these near-source and receiver functions by solving a set of linear equations at each frequency, without assuming any particular parameterization. The near-source term of a particular earthquake reflects spectral differences associated with the rupture process and common to all paths traversed from the earthquake to the arrays, which differ from the regional average. Because paths from all earthquakes cross common structure in the uppermost 15–20 km, the latter must be due to attenuation differences within the structure below these depths.

[10] Details of our estimation procedure are explained as follows. We record the displacement time series, $u(t,j,k,n)$, for $j = 1\ldots J$ earthquakes on $k = 1\ldots K$ arrays. We assume that the S-wave seismogram - the displacement spectrum of the jth earthquake at the nth station of the kth array - may be expressed as a product of a source, propagation, and receiver term. Because the stations within a single array are so closely spaced we can further assume that the propagation to all stations within a single array is the same, and write the displacement spectrum, as

$$U(f)^k_{j,n} = S(f)_j \times P(f)^k_j \times R(f)^k_n \quad (1)$$

$S(f)$, $P(f)$ and $R(f)$ represent source, propagation and receiver terms, respectively, all of which vary with frequency, f. This becomes a sum if we take the logarithm, or

$$\log U(f)^k_{j,n} = \log S(f)_j + \log P(f)^k_j + \log R(f)^k_n \quad (2)$$

If all stations recorded all earthquakes, there would be $J \times \Sigma_{k=1}^{K} N(k)$ observations constraining $(K + 1)J \times \Sigma_{k=1}^{K} N(k)$ unknowns (i.e., J source terms, $K \times J$ propagation terms, and $\Sigma_{k=1}^{K} N(k)$ receiver terms).

[11] Although the number of observations well exceeds the number of unknowns, the close spacing of the stations within each array implies they are likely not independent. Thus, we reduce the number of unknowns by assuming propagation may be described by simple spreading and attenuation functions, of the form

$$1/r \; e^{-\gamma r f} \quad \text{with} \gamma = \pi/\beta Q \quad (3)$$

in which r is hypocentral distance, β is the shear velocity, and Q is a single, regionally averaged quality factor. Substituting this into equation (2) yields the linear equation describing a single measurement

$$\log U(f)^k_{j,n} = \log S(f)_j - \log\left(r^k_j\right) - (\gamma/2.3) r^k_j f + \log R(f)^k_n \quad (4)$$

or putting the known quantities on the left side of the equality:

$$\log U(f)^k_{j,n} + \log\left(r^k_j\right) = \log S(f)_j - (\gamma/2.3) r^k_j f + \log R(f)^k_n \quad (5)$$

Thus, we reduce the $K \times J$ propagation terms to a single unknown, γ, that we assume is independent of frequency. In addition, there is an unknown absolute scaling for all seismograms (e.g., from counts to ground displacement) and for the size of each earthquake that is independent of frequency. These can be combined into a single unknown, C_j, for each source and equation (5) becomes

$$\log U(f)^k_{j,n} + \log\left(r^k_j\right) = C_j + \log \Sigma(f)_j - (\gamma/2.3) r^k_j f + \log R(f)^k_n \quad (6)$$

in which Σ is a normalized version of S, describing just the shape of the source spectrum.

[12] Our task now involves solving for $j = 1,\ldots J$ near-source and $n = 1,\ldots \Sigma_{k=1}^{K} N(k)$ site terms, constrained by $J \times \Sigma_{k=1}^{K} N(k)$ spectral measurements at each frequency. To make

Figure 2. Example N-S seismograms and map view of epicenters and 30-km-depth P wave velocity model. The map shows array locations (black squares) and epicenters of 37 events studied with white circles and triangles for events that have lower and higher frequency content (see Figure 3) respectively, labels denote event index numbers keyed to Table 1, and solid symbols and asterisks next to event numbers indicate repeating events (seismograms of repeats not shown, except events 10 and 11, 9 and 13). These are superposed on a tomographic image of the P wave velocity structure and the location of plate interface (white line) at 30 km depth, both from *Preston* [2003]. Note that this interface model differs from that of *McCrory et al.* [2006] in Figure 1. The waveform for each event from station BH04 of the BH array (selected because it recorded all events except Event 32) is shown, scaled to its peak amplitude, also labeled with event numbers. Waveforms of events in the northern half are above the image and from the southern half below, in the western, central and eastern thirds in the left, center and right columns respectively, and in latitude order from top to bottom. Note the similarity in waveforms of seismograms of sources within 10 km of one another, indicated by similarly aligned event numbers positioned toward the waveforms' centers. Also striking is the correlation of frequency content with epicentral location, with the lowest frequency waveforms from sources in the southeastern quadrant.

solution of equation (6) computationally feasible we solve first for frequency-independent parameters C_j and γ. In other words, we fit as much of the observed spectra as possible with simple linear fits, in which the slope represents a single, regionally averaged attenuation parameter and the intercepts represent the $J + 1$ unknowns describing the different source sizes plus a constant scaling common to all the data. Mathematically this corresponds to solving equation (6) sequentially, first solving the linear equation for the frequency-independent parameters using all data at all frequencies. Mathematically, we first solve

$$\log U(f)_{j,n}^{k} + \log\left(r_j^k\right) \approx C_j - (\gamma/2.3) r_j^k f \tag{7}$$

for all frequencies. We then remove this from the data and ascribe the remaining signal to the source spectrum and site response. Next, at each frequency we solve

$$\log U(f)_{j,n}^{k} + \log\left(r_j^k\right) - C_j + (\gamma/2.3) r_j^k f = \log \Sigma(f)_j + \log R(f)_n^k \tag{8}$$

It is important to note that for each earthquake the portion of the spectrum that is common to all arrays is modeled by the source term, $\log\Sigma(f)$. This means that any propagation affects that were shared by all paths for a particular earthquake, but differed from the regional average propagation, would be included in the source term.

3.2. Near-Source Spectra

[13] The spectral modeling reveals variations in near-source spectral shapes that correlate remarkably with P- and S-velocity structure imaged by *Preston* [2003] and corroborated by other studies [*Rondenay et al.*, 2001; *Abers et al.*, 2009; *Calkins et al.*, 2011; *Calvert et al.*, 2011]. Displacement spectra of waves that traversed a marked low-velocity zone have systematically more negative slopes than those traveling through higher velocity material (Figure 3). Events 2 and 35 are exceptions to this, but the spectra of Event 35 and those of events 36 and 37 are suspect as the signals are barely above the pre-event backgrounds, which have similar spectral decay rates as the signals (see Figure S1 of the auxiliary material). Event 2 was grouped with Events 4 and 20 because they are within 10 km of one another, but of all events its path is the most marginal between the low and higher velocity zones (Figure 3) and thus reasonably could be identified with the other events that have negative spectral slopes. The low velocities are likely signatures of sediments that have been subducted and underplated beneath the higher-velocity Crescent terrane of the North American plate, and of trapped fluids released during eclogite metamorphism of the oceanic crust [*Preston*, 2003; *Calkins et al.*, 2011; *Calvert et al.*, 2011]. In southwest Japan LFE's and earthquakes have been inferred to locate below and on the plate boundary, respectively [*Shelly et al.*, 2006], and distribution of focal depths shown in Figure 3 appears to have the opposite relationship to the plate interface. However, the latter is suggestive at best, as it may reflect location biases (a single 1-D velocity model was used to locate all events) and moreover, the location of the Cascadia plate boundary remains poorly determined (evident by comparing the models of *McCrory et al.* [2006] in Figure 1 and *Preston* [2003] in Figure 3).

[14] That spectra for sources separated by only a few tens of km are nearly identical indicates both a strong dependence on near-source structure and that the near-source structure is fairly continuous on the scale of the earthquake separation. The similarity of the spectra also indicates the small events may have source durations short enough to be considered impulses for the frequencies considered, as discussed in more detail in section 4. These correlations may be confirmed directly from the variations in unprocessed waveforms (Figure 2), providing confidence in our spectral analysis results.

[15] The correlations between the variations in near-source spectral slopes and in seismic structure lead us to conclude that the slope variations reflect attenuation differences below ~20 km depth, because propagation paths above this depth sample the same structure. The slope differences may be explained by plausible attenuation changes (see section 3.3) and notably, exceed differences expected between models of slow slip and earthquake sources (Figure 3).

3.3. Propagation Spectra and Attenuation

[16] The slope fit to all the spectra, or γ in equation (7), is consistent with a regionally averaged quality factor of $Q_S \sim 200$, in line with previously published estimates [*Erickson et al.*, 2004; *Fatehi and Herrmann*, 2008; *Phillips and Stead*, 2008]. Of greater significance however, are answers to the questions of whether variations in spectral slopes could be due to local variations in attenuation, and if so, how large these variations need to be to explain the observations? We address these questions assuming the same description of the attenuation as in equation (3), but now allowing for a portion of the propagation path, Δr, to pass through a region with a different Q value that we denote as Q_2. In other words, the displacement attenuates according to

$$U(f)\alpha\, e^{-\pi f}/\beta[(r-\Delta r)/Q + \Delta r/Q_2] = e^{-\pi f}/\beta Q[r + \Delta r(Q/Q_2 - 1)] \tag{9}$$

Since we are considering the variation from the regionally averaged attenuation, or the difference from (the first exponential term in equation (9))

$$U(f)e^{\gamma f r} = U'(f)$$

the spectrum we measure is described by the second term, or

$$U'(f)\alpha\, e^{-\gamma f \Delta r}(Q/Q_2 - 1) \tag{10}$$

Thus over a frequency interval $\Delta f > 0$ we expect the logarithm of spectral amplitude $U'(f)$ to decrease according to

$$\Delta \log U' = (\gamma \Delta f \Delta r/2.3)(Q/Q_2 - 1) \tag{11}$$

Rearranging we find the change in Q needed over Δr to explain the spectral slope variations, or

$$Q_2/Q = [1 - 2.3/(\gamma \Delta f \Delta r)\Delta \log U']^{-1} \tag{12}$$

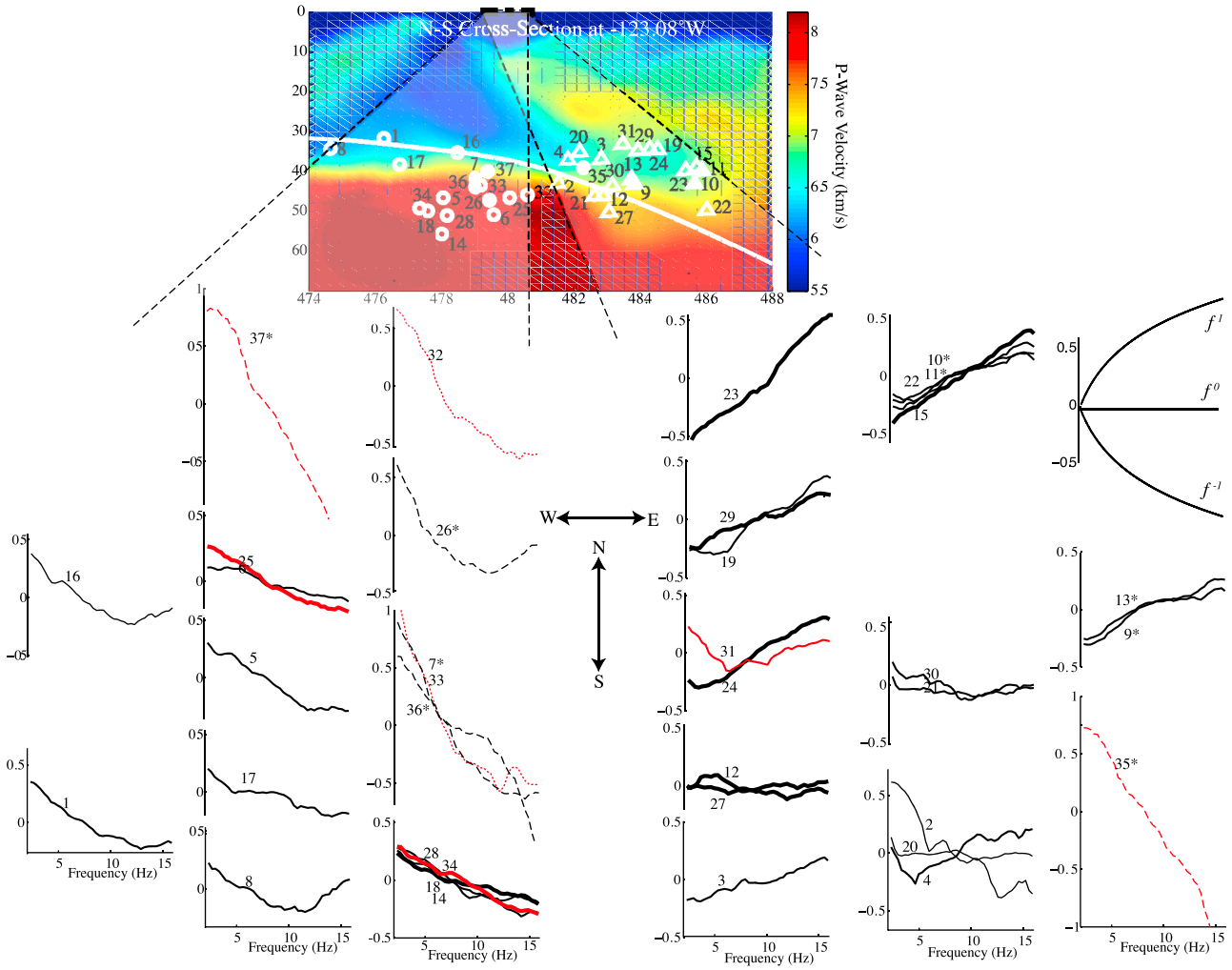

Figure 3. Near-source displacement spectra and P wave velocity cross-sectional image. Symbols and labeling as in Figure 1. (top) Tomographic cross-section of the P wave velocity structure along a N-S cross-section and the plate interface location (white curve) at 123°W from *Preston* [2003] with superimposed array locations and hypocenters of 37 events studied. (bottom) Near-source spectra shown estimated from the logarithm of spectral amplitudes measured for 3-s S-wave windows of E-W component seismograms. Spectra are ordered geographically as in Figure 1; those plotted on the left half correspond to events with propagation paths that pass through the low velocity zone (southern transparent swath). Spectra plotted on the right half with paths largely outside the low velocity zone (northern transparent swath in cross-section). Exceptions to the correlation between spectral slope and path are Events 2 and 35, explained in the text. Theoretical curves showing decay rates of f, f^0, and f^{-1}, are shown for reference in the column on the right. Vertical axes are logarithmic and units are all identical but arbitrary, because the spectra have been normalized by any instrumental absolute scaling (the same for all data) and event sizes (see section 3.1). Spectra are plotted together if from events separated by no more than 10 km. Line types indicate measurement qualities noted in Table 1; qualities 1 = thickest solid, 2 = medium thickness solid, 3 = thinnest sold, 4 = dashed, 5 = dotted. Spectra of events with qualities 4 and 5 likely are contaminated by background noise, as they have the same slopes as a 3-s pre-event sample. Spectra for events during tremor episodes (see Figure 6) are shown in red.

We assess whether a change in Q may explain the observations by calculating this ratio for parameter values based on them. For example, the observations suggest that $\Delta f \sim 10$ Hz and $\Delta \log U' \sim -1$ over a distance $\Delta r \sim 20$ km. Our data fitting yields a value of $\gamma \sim 0043$ (corresponding to $Q \sim 233$) implying from equation (12) that the Q within Δr would need to be ~27% of the regional value, which is low but plausible.

3.4. Site Spectra

[17] The site response functions among stations within a single array vary in a few cases by factors of 3 or more (Figure 4), but qualitatively are consistent with features in the local geology and topography (e.g., the CL array has the most uniform local geology and site response functions, Figure 1). The variation in site response functions agrees

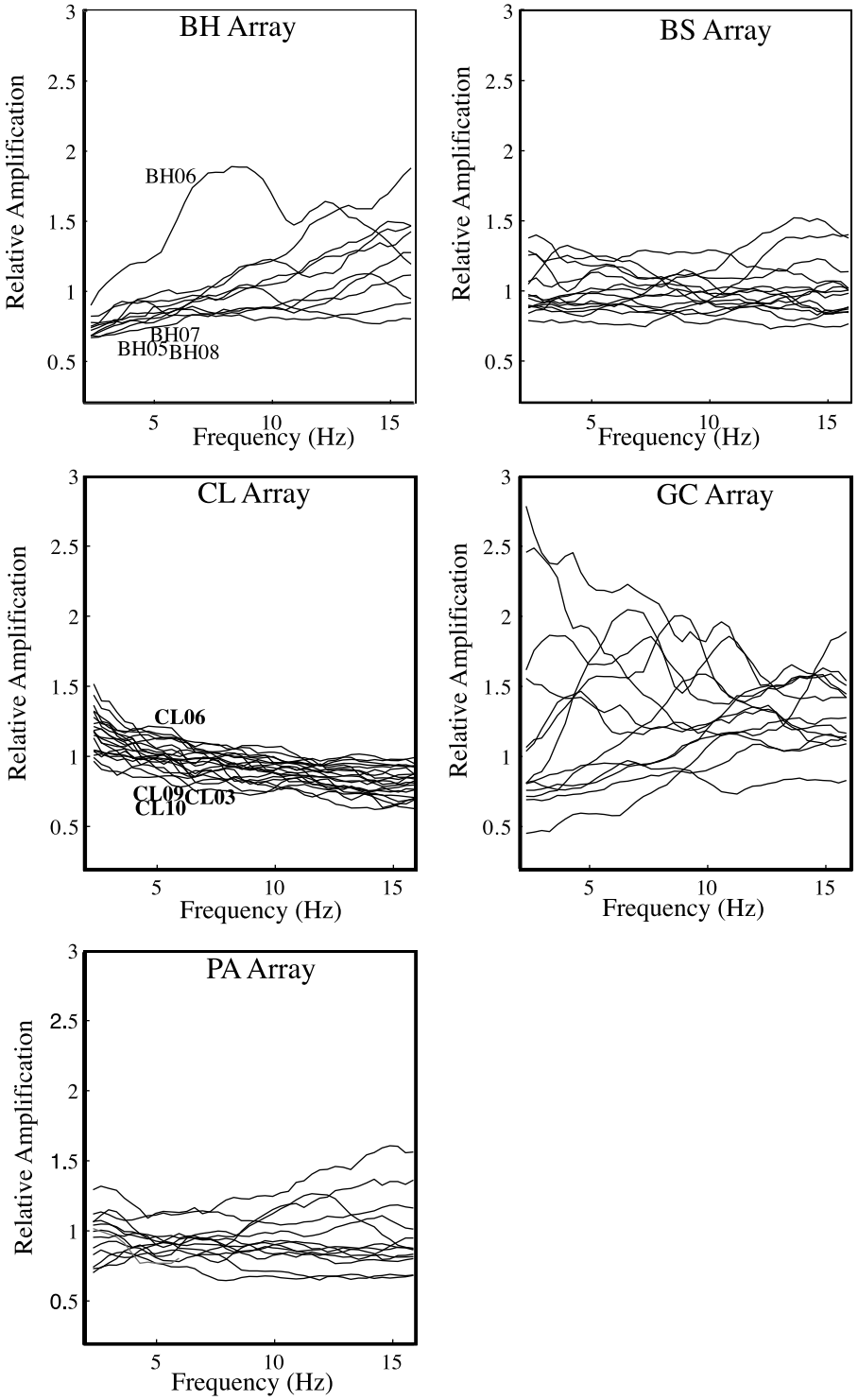

Figure 4. Site-response functions. Linear site amplification estimated at each frequency for each station of each array, estimated with smoothness constraints imposed that minimized the amplitude of the amplification. We labeled the site response functions at 5 Hz for the stations of the BH and CL arrays with the largest and smallest waveforms shown in Figure 5 for two events. Although variable with frequency, these correspond to sites among those with greatest and least overall amplifications, respectively, providing verification of the estimated site response functions.

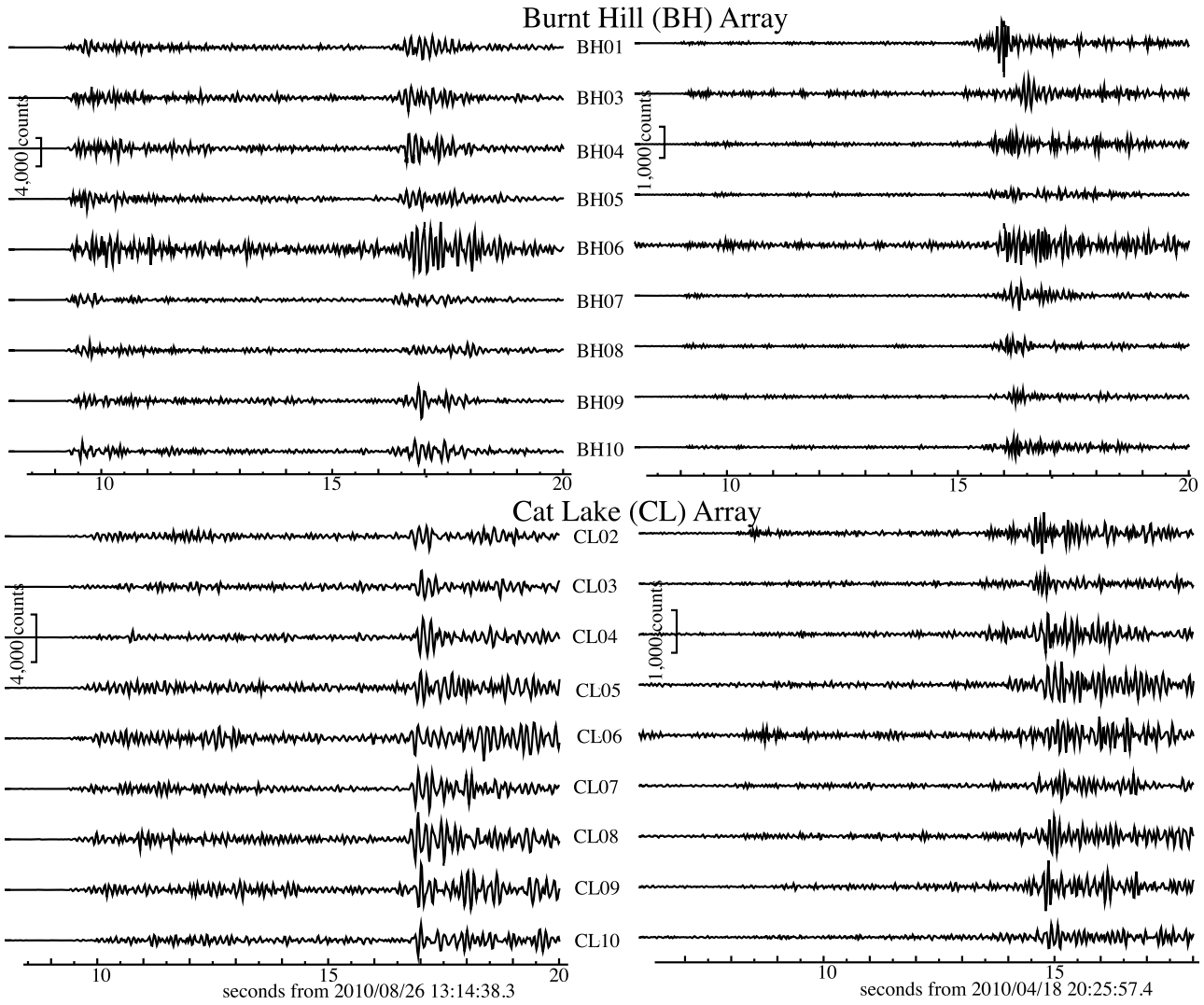

Figure 5. Waveforms of two events (origin times listed at the bottom) recorded on the Burnt Hill and Cat Lake arrays. For each event and array, all waveforms are scaled to the peak of the entire suite.

with what visual examination of the waveforms qualitatively shows. Figure 5 shows the waveforms of two events recorded on two of the arrays. The amplitudes of the waveforms for a single event recorded at the Burnt Hill array vary among the different stations by factors of three or more, with the same variation seen for both events. For example, note that waveform amplitudes at BH06 are largest and at BH05 among the smallest for both events, also consistent with the site response functions (Figure 4). The waveforms recorded at the Cat Lake array are less variable among the different stations, as are the site response functions for this array. Additionally, all the waveforms on the Cat Lake array appear to have longer durations than those recorded at the Burnt Hill array, highlighting the importance of accounting for site response.

[18] The only smoothness constraints imposed in our fitting were applied to site-response functions, and these constraints affected only the absolute amplitudes of the site-response but had insignificant impact on any of the spectral shapes. While site response varied significantly from site to site within a single array, stacking procedures that account for these variations have proven highly effective at reducing noise levels [*Ghosh et al.*, 2010].

4. Source Inferences

4.1. Spectral Shapes

[19] The remarkable correlations between spectral shape and imaged P wave velocity are not likely chance coincidence. We infer that much of the variability in near-source spectra also does not reflect systematic differences in source processes. Moreover, we suggest that most of the events studied are more like earthquakes than slow slip sources. We base this last inference on shapes of the spectra and their variation with event size, interpreted in terms of the aforementioned source and attenuation models. The attenuation model predicts an exponential decrease in spectral amplitude with f. Alternatively, models of source spectra vary as f^n for $f > f_c$ with n depending on the source type, are flat for $f < f_c$ for all source types, and f_c decreases with source size. A distinguishing feature of slow slip events seems to be lower corner frequencies for comparable magnitudes; e.g.,

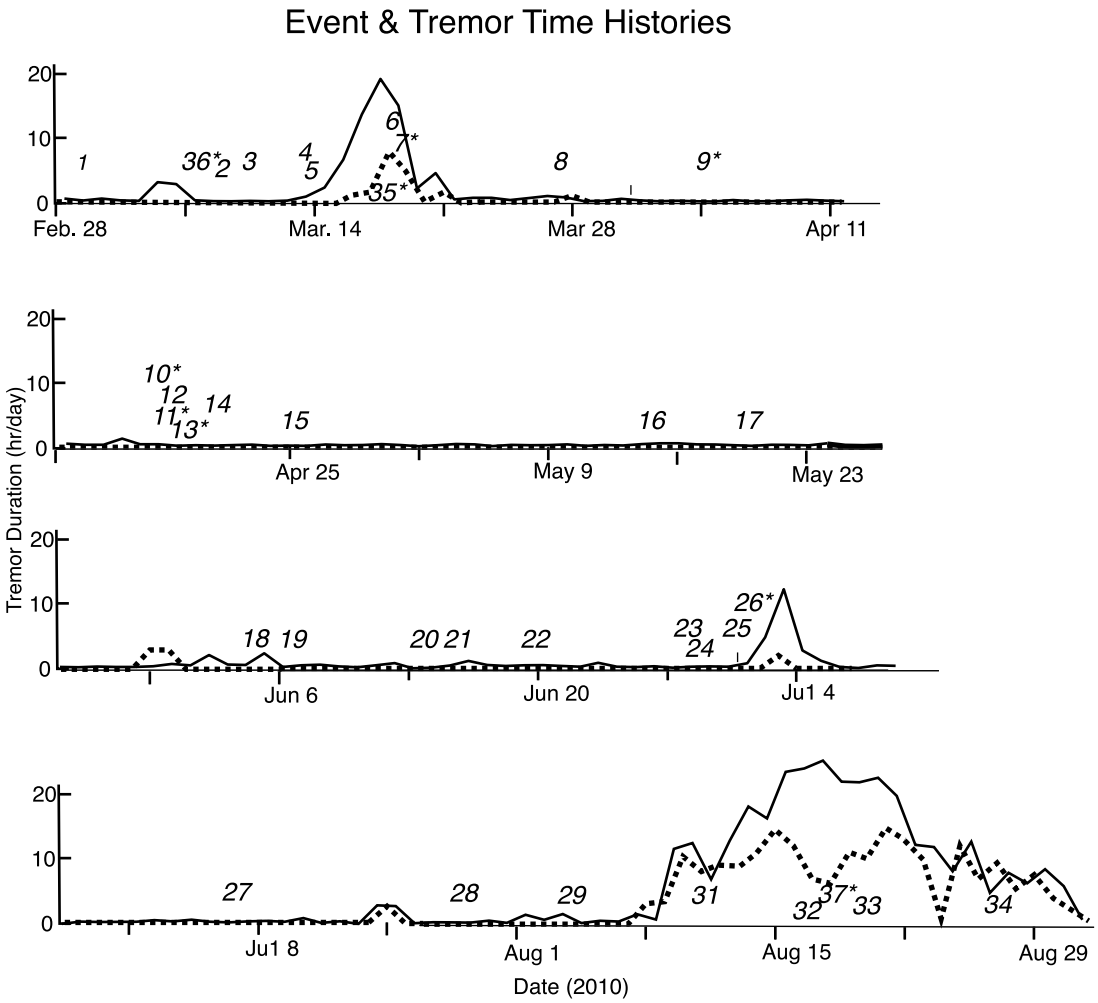

Figure 6. Event and tremor time histories. Tremor activity in northern Washington is detected using the automated system described in *Wech* [2010] (dotted) and A. Ghosh et al. (submitted manuscript, 2012) (solid lines); the *y* axis notes the hours of tremor detected each day. Italicized numbers correspond to the event numbers in Table 1 and Figures 2 and 3, plotted at the origin time of each event and with asterisks indicating repeating events.

Fletcher and McGarr [2011] found $f_c \sim 3$ to 7 Hz for *M*1.6 to *M*1.9 tremor signals recorded in California and *Zhang et al.* [2011] found $f_c \sim 3$ to 8 Hz for Cascadia tremor. In contrast, two studies of *M*1.5 to *M*3.1 and *M*1.0 to *M*4.2 earthquakes in California, f_c varied systematically with magnitude from 5 to 17 Hz and 4 to 55 Hz, respectively [*Shearer et al.*, 2006; *Hardebeck and Aron*, 2009].

[20] If the signals we analyze had corner frequencies similar to those estimated for tremor elsewhere, we would expect at least some of them to fall within our 2 to 16 Hz bandwidth. Several observations violate this expectation and thus support an inferred corner frequency above 16 Hz, noting that the signal cannot be resolved from the noise above this frequency. First, because we plot the spectra on log linear axes in Figure 3, spectra that appear linear would be more consistent with the decay predicted by the assumed attenuation model. Deviations from linearity might also imply a frequency-dependent *Q*, as suggested in one study of attenuation for all of the Pacific Northwest [*Fatehi and Herrmann*, 2008]. If reflecting source processes the spectra would appear curved in Figure 3 for $f > f_c$ and linear for $f < f_c$, with an abrupt decrease in slope if f_c was within the bandwidth. Most of the near-source spectra are adequately fit with a straight line, particularly given the low signal-to-noise ratio in many cases (especially at higher frequencies and below the L-28 sensor natural frequency at 4.5 Hz). Possible exceptions to this may be events 9, 10, 11, 13 and 22.

[21] The second line of evidence that $f_c > 16$ Hz is that near-source spectral shapes are nearly identical for clustered events for which propagation paths are nearly identical but event sizes span several units. Noting that f_c varies theoretically as $10^{-M/2}$ [*Madariaga*, 1976], for this range of magnitudes corner frequencies should differ by a factor of ten or more. Thus unless $f_c > 16$ Hz for all the events we would observe at least a few events with corner frequencies within our 6 to 16 Hz bandwidth. The latter is not the case, noting that for example, the peak amplitudes of waveforms from the cluster of events 14, 18, 28, 34 differ by more than several orders of magnitude (see Table 1) yet the spectral shapes are nearly identical. A simple explanation for the absence of such observations is that all events we studied ruptured like garden-variety earthquakes with $f_c > 16$ Hz,

consistent with their small magnitudes and earthquake observations elsewhere.

4.2. Repeating Events and Relationships to Tremor

[22] We note that 24% of the events studied, some of which were initially classified as earthquakes, appear to have another hallmark feature of LFEs – they repeat on time scales of days to years (based on waveform similarity). However, only 5 of the 9 repeating events have spectral decay rates that would have led to their classification as LFEs (Figure 3). We also note that both repeating and non-repeating events occur during episodes of tremor activity as well as in between these episodes. In Figure 6 we compare the origin times of our 37 events with tremor activity detected in northern Washington by *Wech* [2010] and A. Ghosh et al. (Asperities in the transition zone control the evolution of slow earthquakes, submitted to *Journal of Geophysical Research*, 2012). This figure shows no tremor detected around the time of repeating event 9 and only weak, background levels of tremor (detected only by A. Ghosh et al., submitted manuscript, 2012) around repeating events 10, 11 and 13, but other repeating events occur during episodes of strong tremor. Similarly, no correlation exists between spectral decay rate and whether events occur during intervals of measurable tremor activity; e.g. in Figure 3 note that event 34 (red curve) during an ETS episode has the same spectral decay as Events 14, 18, and 28 (black curves) that occurred when no tremor was detected (Figure 6).

[23] These and the inference in section 4.1 that all events may be earthquakes suggests that some LFEs thought to comprise tremor may be repeating earthquakes with radiated seismic energy depleted in high frequencies due to near-source attenuation. The fact that, as in Cascadia, slow slip phenomena often occur in regions with heterogeneous seismic velocity and other material properties, localized fluids and high pressures, active dehydration and other metamorphic reactions, [*Shelly et al.*, 2006; *Kato et al.*, 2010; *Peng and Gomberg*, 2010; *Brantut et al.*, 2011; *Fagereng and Diener*, 2011] further suggests that consideration of near-source attenuation is warranted.

5. Conclusions

[24] This study alone does not permit us to draw definitive conclusions about other studies elsewhere. However, we conclude that to distinguish "normal" and "slow slip" source process differences for a collection of events, their hypocenters must differ by less than a few tens of km or the potential for near-source attenuation differences should be considered and accounted for. We note that in most cases the distributions of tremor and earthquake sources are anti-correlated [*Peng and Gomberg*, 2010] with separations sufficient to suggest that the attenuation needs consideration as an explanation of spectral differences. Even separations of "closely located" or "nearby" tremor and earthquake sources in studies analyzing spectra to infer source characteristics. [*Rubinstein et al.*, 2007; *Fletcher and Baker*, 2010; *Fletcher and McGarr*, 2011; *Kim et al.*, 2011; *Zhang et al.*, 2011] are sufficiently large to merit consideration of path differences.

[25] We also conclude that ordinary earthquakes and LFEs may not separate so neatly into two, mutually exclusive populations. Earthquakes identified by temporally isolated wave trains with clear P- and S-waves may repeat and LFEs also repeat, both within and outside intervals of tremor activity. Neither the repeating (or lack of) nature of events or their occurrence during or outside tremor correlates with spectral decay rate. However, as noted above, spectral decay rates do vary systematically with source location and correlate clearly with the P wave velocity within tens of km of the hypocenters and thus probably with near-source attenuation.

[26] **Acknowledgments.** The authors thank Honn Kao, Michael Bostock, Art McGarr, Elizabeth Cochran, Craig Weaver, and an anonymous reviewer for thoughtful reviews of this paper. We also thank all those who funded and helped to install and maintain the Array of Arrays and to assemble the data.

References

Abers, G. A., L. S. Mackenzie, S. Rondenay, Z. Zhang, A. G. Wech, and K. C. Creager (2009), Imaging the source region of Cascadia tremor and intermediated-depth earthquakes, *Geology*, *37*, 1119–1122, doi:10.1130/G30143A.1.

Andrews, D. J. (1986), Objective determination of source parameters and similarity of earthquakes of different sizes, in *Earthquake Source Mechanics*, *Geophys. Monogr. Ser.*, vol. 37, edited by S. Das et al., pp. 259–267, AGU, Washington, D. C., doi:10.1029/GM037p0259.

Brantut, N., J. Sulem, and A. Schubnel (2011), Effect of dehydration reactions on earthquake nucleation: Stable sliding, slow transients, and unstable slip, *J. Geophys. Res.*, *116*, B05304, doi:10.1029/2010JB007876.

Brown, J. R., G. C. Beroza, S. Ide, K. Ohta, D. R. Shelly, S. Y. Schwartz, W. Rabbel, M. Thorwart, and H. Kao (2009), Deep low-frequency earthquakes in tremor localize to the plate interface in multiple subduction zones, *Geophys. Res. Lett.*, *36*, L19306, doi:10.1029/2009GL040027.

Brune, J. (1970), Tectonic stress and the spectra of seismic shear waves from earthquakes, *J. Geophys. Res.*, *75*, 4997–5009, doi:10.1029/JB075i026p04997.

Calkins, J. A., G. A. Abers, G. Ekström, K. C. Creager, and S. Rondenay (2011), Shallow structure of the Cascadia subduction zone beneath western Washington from spectral ambient noise correlation, *J. Geophys. Res.*, *116*, B07302, doi:10.1029/2010JB007657.

Calvert, A. J., L. A. Preston, and A. M. Farahbod (2011), Sedimentary underplating at the Cascadia mantle-wedge corner revealed by seismic imaging, *Nat. Geosci.*, *4*, 545–548, doi:10.1038/ngeo1195.

Chen, X., and P. M. Shearer (2011), Comprehensive analysis of earthquake source spectra and swarms in the Salton Trough, California, *J. Geophys. Res.*, *116*, B09309, doi:10.1029/2011JB008263.

Erickson, D., D. E. McNamara, and H. M. Benz (2004), Frequency-dependent Lg Q within the continental United States, *Bull. Seismol. Soc. Am.*, *94*, 1630–1643, doi:10.1785/012003218.

Fagereng, Å., and J. F. A. Diener (2011), Non-volcanic tremor and discontinuous slab dehydration, *Geophys. Res. Lett.*, *38*, L15302, doi:10.1029/2011GL048214.

Fatehi, A., and R. B. Herrmann (2008), High-frequency ground-motion scaling in the Pacific Northwest and in Northern and Central California, *Bull. Seismol. Soc. Am.*, *98*, 709–721.

Fletcher, J. B., and L. M. Baker (2010), Analysis of nonvolcanic tremor on the San Andreas fault near Parkfield, CA using U.S. Geological Survey Parkfield Seismic Array, *J. Geophys. Res.*, *115*, B10305, doi:10.1029/2010JB007511.

Fletcher, J. B., and A. McGarr (2011), Moments, magnitudes, and radiated energies of non-volcanic tremor near Cholame, CA, from ground motion spectra at UPSAR, *Geophys. Res. Lett.*, *38*, L16314, doi:10.1029/2011GL048636.

Ghosh, A., J. E. Vidale, J. R. Sweet, K. C. Creager, A. G. Wech, and H. Houston (2010), Tremor bands sweep Cascadia, *Geophys. Res. Lett.*, *37*, L08301, doi:10.1029/2009GL042301.

Hardebeck, J. L., and A. Aron (2009), Earthquake stress drops and inferred fault strength on the Hayward fault, east San Francisco Bay, California, *Bull. Seismol. Soc. Am.*, *99*, 1801–1814, doi:10.1785/0120080242.

Ide, S. (2010), Quantifying the time function of nonvolcanic tremor based on a stochastic model, *J. Geophys. Res.*, *115*, B08313, doi:10.1029/2009JB000829.

Ide, S., G. C. Beroza, D. R. Shelly, and T. Uchide (2007), A scaling law for slow earthquakes, *Nature*, *447*, 76–79, doi:10.1038/nature05780.

Ito, Y., K. Obara, K. Shiomi, S. Sekine, and H. Hirose (2007), Slow earthquakes coincident with episodic tremors and slow slip events, *Science*, *315*, 503–506, doi:10.1126/science.1134454.

Kato, A., et al. (2010), Variations of fluid pressure within the subducting oceanic crust and slow earthquakes, *Geophys. Res. Lett.*, *37*, L14310, doi:10.1029/2010GL043723.

Kim, M. J., S. Y. Schwartz, and S. Bannister (2011), Non-volcanic tremor associated with the March 2010 Gisborne slow slip event at the Hikurangi subduction margin, New Zealand, *Geophys. Res. Lett.*, *38*, L14301, doi:10.1029/2011GL048400.

Madariaga, R. (1976), Dynamics of an expanding circular fault, *Bull. Seismol. Soc. Am.*, *66*, 639–666.

McCrory, P. A., J. L. Blair, D. H. Oppenheimer, and S. R. Walter (2006), Depth to the Juan de Fuca slab beneath the Cascadia subduction margin: A 3-D model for sorting earthquakes, *U.S. Geol. Surv. Data Ser.*, *91*.

Peng, Z., and J. Gomberg (2010), An integrated perspective of the continuum between earthquakes and slow-slip phenomena, *Nat. Geosci.*, *3*, 599–607, doi:10.1038/ngeo940.

Phillips, W. S., and R. J. Stead (2008), Attenuation of Lg in the western US, using the USArray, *Geophys. Res. Lett.*, *35*, L07307, doi:10.1029/2007GL032926.

Preston, L. A. (2003), Simultaneous inversion of 3D velocity structure, hypocenter locations, and reflector geometry in Cascadia, PhD thesis, 135 pp., Univ. of Wash., Seattle.

Rondenay, S., M. G. Bostock, and J. Shragge (2001), Multiparameter two-dimensional inversion of scattered teleseismic body waves: 3. Application to the Cascadia 1993 data set, *J. Geophys. Res.*, *106*, 30,795–30,807, doi:10.1029/2000JB000039.

Rubinstein, J. L., J. E. Vidale, J. Gomberg, P. Bodin, K. C. Creager, and S. D. Malone (2007), Non-volcanic tremor driven by large transient shear stresses, *Nature*, *448*, 579–582, doi:10.1038/nature06017.

Shearer, P. M., G. A. Prieto, and E. Hauksson (2006), Comprehensive analysis of earthquake source spectra in southern California, *J. Geophys. Res.*, *111*, B06303, doi:10.1029/2005JB003979.

Shelly, D. R., G. C. Beroza, S. Ide, and S. Nakamula (2006), Low frequency earthquakes in Shikoku, Japan, and their relationship to episodic tremor and slip, *Nature*, *442*, 188–191, doi:10.1038/nature04931.

Shelly, D. R., G. C. Beroza, and S. Ide (2007), Non-volcanic tremor and low-frequency earthquake swarms, *Nature*, *446*, 305–307, doi:10.1038/nature05666.

Sweet, J., K. C. Creager, A. Ghosh, and J. Vidale (2010) Low-frequency earthquakes in Cascadia, Abstract S23A-2090 presented at 2010 Fall Meeting, AGU, San Francisco, Calif., 13–17 Dec.

Vidale, J. E., A. J. Hotovec, A. Ghosh, K. C. Creager, and J. Gomberg (2011), Tiny intraplate earthquakes triggered by nearby episodic tremor and slip in Cascadia, *Geochem. Geophys. Geosyst.*, *12*, Q06005, doi:10.1029/2011GC003559.

Wech, A. G. (2010), Interactive tremor monitoring, *Seismol. Res. Lett.*, *81*, 664–669, doi:10.1785/gssrl.81.4.664.

Zhang, J., P. Gerstoft, P. M. Shearer, H. Yao, J. E. Vidale, H. Houston, and A. Ghosh (2011), Cascadia tremor spectra: Low corner frequencies and earthquake-like high-frequency falloff, *Geochem. Geophys. Geosyst.*, *12*, Q10007, doi:10.1029/2011GC003759.